Journal of Nuclear Medicine, published on September 9, 2021 as doi:10.2967/jnumed.121.262368

^{18}F-BMS986192 PET imaging of PD-L1 in metastatic melanoma patients with brain metastases treated with immune checkpoint inhibitors. A pilot study.

Short Running Title: PET imaging of PD-L1 in melanoma

Authors:

Pieter H. Nienhuis[1], Inês F. Antunes[1], Andor W.J.M. Glaudemans[1], Mathilde Jalving[2], David Leung[3], Walter Noordzij[1], Riemer H.J.A. Slart[1,4], Erik F.J. de Vries[1], Geke A.P. Hospers[2]

Affiliations:

[1]Medical Imaging Center, Department of Nuclear Medicine and Molecular Imaging, University of Groningen, University Medical Center Groningen, The Netherlands; [2]Department of Medical Oncology, University of Groningen, University Medical Center Groningen, The Netherlands; [3]Bristol Myers Squibb, Princeton, NJ, USA; [4]Faculty of Science and Technology, Department of Biomedical Photonic Imaging, University of Twente, Enschede, The Netherlands.

Corresponding Author:

G.A.P. Hospers, MD, PhD
Department of Medical Oncology
University Medical Center Groningen
P.O. Box 30.001
Hanzeplein 1
9700 RB Groningen, The Netherlands
E-mail: g.a.p.hospers@umcg.nl
Telephone: +31 503612821
Fax: +31 503614862

First Author:

Pieter H. Nienhuis

MD/PhD Candidate

Department of Nuclear Medicine and Molecular Imaging

University Medical Center Groningen

Hanzeplein 1

9700 RB Groningen, The Netherlands

E-mail: p.h.nienhuis@umcg.nl

Telephone: +31 50 3617047

Fax: +31503614862

Word count: 5105 words

ABSTRACT

Immune checkpoint inhibitors (ICI) targeting PD-1/PD-L1 frequently induces tumor response in metastatic melanoma patients. However, tumor response often takes months and may be heterogeneous. Consequently, additional local treatment for non-responsive metastases may be needed, especially in the case of brain metastases. Non-invasive imaging may allow the characterization of (brain) metastases to predict response. This pilot study uses 18F-BMS986192 PET for PD-L1 expression to explore the variability in metastatic tracer uptake and its relation to tumor response, with a special focus on brain metastases.

Methods

Metastatic melanoma patients underwent whole-body 18F-BMS986192 PET/CT scanning before and 6 weeks after starting ICI therapy. 18F-BMS986192 uptake was measured in healthy tissues, organs, and tumor lesions. Tumor response was evaluated at 12 weeks using CT thorax/abdomen and MRI brain. RECIST v 1.1 was used to define therapy response per patient. Response per lesion was measured by the percentage change in lesion diameter. Toxicity was assessed according to Common Terminology Criteria for Adverse Events version 4.0.

Results

Baseline 18F-BMS986192 PET/CT was performed in 8 patients, with follow-up scans in 4 patients. The highest tracer uptake was observed in the spleen, bone marrow, kidneys, and liver. Tracer uptake in tumor lesions was heterogeneous. In total, 42 tumor lesions were identified at baseline with most lesions in the lungs (n=21) and brain (n=14). Tracer uptake was similar between tumor locations. 18F-BMS986192 uptake in lesions at baseline, corrected for blood pool activity, was negatively correlated with the change lesion diameter at response evaluation (r=-0.49, p=0.005), both in intra- and extracerebral lesions. Receiver operating characteristic (ROC) analysis demonstrated that 18F-BMS986192 uptake can discriminate between responding and nonresponding lesions with an area under the curve of 0.82. At the follow-up scan an increased 18F-BMS986192 uptake compared to baseline scan was correlated with an

increased lesion diameter at response evaluation. In the follow-up 18F-BMS986192-PET scan of two patients, ICI-related toxicity (thyroiditis and colitis) was detected.

Conclusion

In this pilot study, 18F-BMS986192 PET showed heterogeneous uptake in intra and extracerebral metastatic lesions in melanoma patients. Baseline 18F-BMS986192 uptake was able to predict an ICI treatment-induced reduction in lesion volume, whereas the follow-up PET scan allowed the detection of treatment-induced toxicity.

Keywords:

Positron Emission Tomography, PD-L1 Expression, Metastatic Melanoma, Brain Metastasis, Immune Checkpoint Inhibition

INTRODUCTION

Immune checkpoint inhibitors (ICI) targeting the Programmed cell death protein-1 (PD-1)/Programmed cell death ligand-1 (PD-L1) axis or cytotoxic T-lymphocyte-associated protein 4 (CTLA-4) receptor, either as monotherapy or as combined treatment, have shown response rates of approximately 40 to 60% in patients with metastatic melanoma, with progression-free and overall survival (*1–8*).

However, it often takes months before response to ICI treatment can be detected, and lesions may respond in a heterogeneous manner. Some lesions may respond, while other lesions may not respond or display pseudoprogression (*9*). Consequently, some fast-growing lesions may require additional treatment. Data from the Dutch National Cancer Registry shows that 22% (876/3959) of metastatic melanoma patients underwent surgery for nonresponding metastases in addition to systemic treatment with ICI (*10*). Moreover, approximately 30% of metastatic melanoma patients develop brain metastases. Brain metastases are considered as a risky location because they carry a high risk for developing central nervous system failure and mortality (*11*). Therefore, local treatment with radiotherapy or resection is often considered in patients with brain metastases.

Before starting ICI therapy, it is difficult to determine which lesions will respond and which lesions will require additional treatment. Immunohistochemistry on biopsy samples only provides information about a small fraction of a single tumor lesion, and is, therefore, unable to address intra and intertumoral heterogeneity. This limits the value of immunohistochemistry to predict response. In patients with metastatic melanoma, known to be a high heterogenic responding tumor, PD-1 immunohistochemistry staining on biopsies was not a good predictor of response to ICI, and hence is not used in clinical practice (*12*).

Whole-body positron emission tomography (PET) imaging with a PD-L1 targeting tracer may have added value in detecting heterogenic expression of the drug target for anti-PD-1 therapy. Detection of low levels of PD-L1 expression may be predictive for nonresponding lesions that will require additional

treatment. PET imaging of PD-L1 expression in non-small cell lung cancer, bladder weecancer, and triple-negative breast cancer has shown that the intensity of the PET signal correlates with tumor response to ICI (*13*,*14*). The same approach could also be used to address the heterogeneity of metastatic tumor lesions in melanoma. This might especially be of importance for the characterization of brain lesions. PET imaging of PD-L1 expression may thus be a viable non-invasive diagnostic tool for lesion characterization and response prediction in metastatic melanoma patients.

This pilot study investigated the intensity and variability of PD-L1 expression using 18F-BMS986192 PET in metastatic tumor lesions of melanoma patients, including patients with brain metastases. As secondary objectives, we explored whether 18F-BMS986192 uptake was related to tumor response and whether enhanced tracer uptake in major organs was related to immune-related toxicity.

MATERIALS AND METHODS

Patient Population

Patients ≥ 18 years with stage IV metastatic melanoma who were eligible for treatment with ICI were recruited into the study. Patients with brain metastases were preferably included. Patients with suspected brain metastases could be treated with stereotactic radiotherapy prior to start of the ICI therapy, however these irradiated lesions were not included in the analyses. Other inclusion criteria were the presence of measurable disease according to RECIST v1.1, an Eastern Cooperative Oncology Group performance status of 0–1, and an adequate hematologic and end-organ function (*15*). The main exclusion criteria were pre-existing autoimmune disease and treatment with immunosuppressive medication.

This study was approved by the Medical Ethical Committee (METc) of the University Medical Center Groningen (UMCG), delegated by the Central Committee on Research Involving Human Subjects, and was registered at ClinicalTrials.gov (ClinicalTrials.gov Identifier: NCT03520634) and METC 2016/646 (EUDRACT Number 2015-004920-67 with site-specific amendment 6). All patients provided written informed consent.

Study Design

This single-center imaging study with the 18F-BMS986192 tracer was performed at the UMCG, the Netherlands. Patients received either nivolumab (anti-PD-1) or a combination of nivolumab and ipilimumab (anti-CTLA-4). The combination therapy consisted of 4 cycles of ipilimumab and nivolumab every 3 weeks, followed by nivolumab monotherapy. Included patients were all treated with an ICI. The study intervention was a 18F-BMS986192 PET scan at baseline and 6 weeks after treatment initiation.

Production of 18F-BMS-986192

The azide precursor BMT-180478 and the adnectin BMT-192920, both required for the on-site preparation of the PET tracer 18F-BMS986192, were kindly provided by Brystol Myers Squibb (Supplemental Fig. 1). The final PET tracer 18F-BMS-986192 was produced in a GMP compliant automated synthesis module according to the previously published protocol (*16*). The radiochemical purity of 18F-BMS986192 was always >95% and the molar activity always exceeded 3.000 GBq/mmol.

18F-BMS-986192 PET Acquisition and Analysis

Patients received an intravenous bolus injection of approximately 185 MBq (range 182-192 MBq) 18F-BMS986192. PET image acquisition followed 60 minutes after tracer injection on a Biograph mCT64 or mCT40 camera (Siemens Medical Systems, Knoxville, TN, USA). Whole-body PET scans (head to toe; 12 bed positions, 3 minutes per bed position) were acquired together with a low dose CT scan. Vital signs (blood pressure and heart rate) were measured before, 10 minutes after the injection of 18F-BMS986192, and immediately after the PET-CT scan. Patients remained under observation for 120 minutes after tracer injection.

All PET scans were reconstructed according to the EARL criteria and analyzed using Syngo.via VB30 software (Siemens) (*17*). For quantification of 18F-BMS986192 uptake, volumes of interest (VOI) were manually drawn (AWJMG, PHN) around the visible tumor lesions in the PET scan. For PET-negative lesions, the VOI was drawn around the tumor lesion on the CT or MRI scan that was manually aligned with the PET scan.

Tracer uptake in healthy tissues and lymphoid tissues (lung, thoracic aorta, spleen, liver, bone marrow, tonsils, parotid glands, thyroid, and axillary and inguinal lymph nodes) was measured to assess any toxicity-related increase in tracer uptake, using manually drawn VOIs. Tracer uptake was corrected for body weight and injected dose and expressed as standardized uptake values (SUV_{max}, SUV_{mean}, and SUV_{peak} for tumor lesions and SUV_{mean} for normal tissues) consistent with EANM guidelines for ^{18}F tracers in tumors

(*18*). Because the SUV may be influenced by patient-specific characteristics, such as tracer metabolism and clearance, tumor-to-blood ratios (TBR) were calculated using the VOI of the lesion and the thoracic aorta ($TBR = \frac{Tumour\ SUV}{Blood\ Pool\ SUVmean}$) (*19*).

Response Evaluation

Response to therapy was evaluated according to RECIST v1.1 (*15*). Contrast-enhanced chest-abdominal CT and Gadolinium-enhanced MRI brain scans were performed at baseline and week 12 as part of routine patient care.

Tumor lesions that were scanned on MR or CT at baseline but not at follow up were excluded from response evaluation. To evaluate response per tumor lesion, the percentage change of the diameter at follow-up compared to baseline was calculated (WN, PHN). Tumor lesions with a long-axis diameter smaller than 10 mm and lymph node lesions with a short-axis diameter smaller than 15 mm were excluded from response analysis.

Adverse events induced by the ICI treatment were assessed at each outpatient visit, using the National Cancer Institute Common Terminology Criteria for Adverse Events version 4.0 and reported in this study until the 12-week tumor response evaluation.

Statistical Analyses

Patients were evaluated for tracer biodistribution analysis if they underwent at least one 18F-BMS986192 PET scan. An assessment of the normality of data was performed using the Shapiro-Wilk test. Differences in tracer uptake between the baseline and on-treatment 18F-BMS986192 PET scans were analyzed using a Paired T-test. Correlations between parameters were calculated using the Spearman correlation test. *P* values <0.05 were considered statistically significant. PET data are expressed as median with interquartile range (IQR) for non-normally distributed data and are expressed as mean with standard deviation (SD) for normally distributed data.

Receiver operating characteristic (ROC) analyses were calculated to determine the 18F-BMS986192 uptake value that best differentiates between responding and nonresponding lesions. Statistical analyses were performed using GraphPad Prism 8.0.1 software for Microsoft Windows.

RESULTS

A total of 10 patients were included in this study, of whom 8 received a baseline 18F-BMS986192 PET/CT imaging before starting anti-PD-1 therapy (Table 1). In the remaining two patients, no PET scans could be performed due to rapid clinical progression. In four patients, the on-treatment 18F-BMS986192 PET/CT scan was performed between 41 and 55 days (mean 42) after starting anti-PD-1 therapy. No 18F-BMS986192-related side effects occurred within the observation period of 120 minutes after tracer injection.

Biodistribution of 18F-BMS986192

The biodistribution of 18F-BMS986192 was evaluated in healthy tissues at baseline. High tracer uptake at baseline was observed in the spleen (SUV_{mean} 15.9±8.7), bone marrow (6.9±1.5), and liver (4.7±2.4). Patients with a follow-up scan (n=4) did not show significant changes in uptake in healthy tissues compared with the baseline PET scan, except for tonsil uptake, which was significantly higher at baseline than at follow up (Wilcoxon Signed Rank Test, p=0.002) (Fig. 1).

Variability in 18F-BMS986192 Uptake In Metastatic Lesions

Of the 42 evaluable tumor lesions, 21 were located in the lungs, 14 in the brain, two in soft-tissue, and one in bone, mediastinum, peritoneum, adrenal gland, and lymph node. Examples of PET images of a brain and lung lesion are depicted in Figure 2. The variability in uptake is shown in Figure 3 and Supplemental Figures 2 and 3. No significant differences were observed in 18F-BMS986192 uptake between lung and brain lesions (p=0.06). One bone lesion was excluded from analyses because its VOI could not be sufficiently separated from the high bone marrow uptake nearby and this resulted in an uptake value 6 standard deviations higher than the other metastatic lesions.

Association between Baseline Tumor Uptake and Response to Therapy

After the exclusion of small tumor lesions (median diameter 5 mm, range 4-9 mm), 32 lesions (8 brain lesions) remained for response evaluation. The percentage change in lesion diameter was not associated with the baseline tracer uptake parameters SUV_{max} (r=-0.15, p=0.42), SUV_{mean} (r=-0.17, p=0.34), or SUV_{peak} (r=-0.18, p=0.31).

When correcting for differences in tracer availability, using the tracer uptake in the blood pool as reference, a significant correlation was observed between baseline tumor-to-blood ratio and change in tumor lesion size (Fig. 4). This negative association was seen when calculating a TBR from the SUV_{max} (r=-0.43, p=0.014), SUV_{mean} (r=-0.44, p=0.012), or SUV_{peak} (r=-0.49, p=0.005) of the tumor and SUV_{mean} of the blood pool. The same negative association was observed when only analyzing the intracerebral (brain) lesions, but this association was statistically not significant (r=-0.54, p=0.17).

Discrimination of Responding and Non-responding Tumors

Receiver operating characteristic (ROC) analysis was performed to assess the optimal tracer uptake value for predicting an ICI-induced reduction in tumor diameter. Using a TBR derived from SUV_{peak} of the lesion and SUV_{mean} of the aortic blood pool, ROC analysis resulted in an area under the curve of 0.82 (p=0.006). Using a TBR cut-off value of 1.3 resulted in a sensitivity of 89% (95% CI 57%-99%) and a specificity of 78% (95% CI 58%-90%) for discriminating a tumor decreasing in size from a tumor increasing in size (Fig. 5).

Follow Up 18F-BMS986192 Scan and Response to Therapy

Four patients (50%) with a total of 19 metastases had a follow-up 18F-BMS986192 scan at 6 weeks. A paired t-test revealed no differences in tumor 18F-BMS986192 uptake between baseline and follow-up scans. Figure 6A shows the individual differences in tumor 18F-BMS986192 uptake between baseline and

follow-up for the brain and lung lesions in these 4 patients. 18F-BMS986192 uptake was significantly lower in the brain lesions compared to the lung lesions, both at baseline and on-treatment (p=0.004 and p=0.05, respectively). No differences were observed in the mean lesion size of these brain and lung lesions.

Fourteen of the 19 metastases on follow-up scans were larger than 10 mm at baseline. A significant correlation between the change in 18F-BMS986192 uptake (TBR) and the change in tumor size between the baseline and follow-up was observed (r=0.79, p=0.0007; Fig. 6B).

Assessment of toxicity: Increased Uptake of 18F-BMS986192

Follow-up 18F-BMS986192 scans were also evaluated for ICI-related toxicity. One patient developed ICI-related hyperthyroidism, another patient colitis. The follow-up PET scan of the patient with ICI-related hyperthyroidism showed increased uptake in the thyroid (Fig. 7). This diagnosis was substantiated by blood TSH levels of 0.007 mU/L (normal 0.5-4 mU/L) and f T4 levels of 37.2 pmol/L (normal 11-19.5 pmol/L). The patient who developed a ICI-related colitis one day after the PET scan did show a different bowel uptake pattern at the second scan compared to the first scan, but solely based on the PET scan a definitive diagnosis of colitis cannot be settled.

DISCUSSION

This is the first study to investigate 18F-BMS986192 PET imaging before and during ICI therapy in patients with metastatic melanoma, including patients with brain metastases. We found heterogeneous uptake of 18F-BMS986192 in metastatic lesions at all locations, which is in line with a heterogeneous response to ICI therapy that is often observed in melanoma patients. Interestingly, we observed that high baseline 18F-BMS986192 uptake in lesions, corrected for blood pool uptake, correlated with response to ICI treatment. The same trend was found for brain lesions, which is an important finding, since non-responding brain lesions often require additional treatment. Additionally, increased 18F-BMS-986192 uptake in tumor lesions at the follow 18F-BMS986192 PET scan at week 6 was correlated with tumor progression at 12 weeks.

Within a single patient with metastatic melanoma, different metastatic lesions may respond variably to ICI therapy. This variability in response to ICI is both in terms of the change in the lesion volume and the time it takes a lesion to show response (*20*). Due to this variability in response to ICI, additional local treatment is often necessary on nonresponding metastatic melanoma lesions (*10*). High immunohistochemistry PD-L1 expression in a metastatic lesion is associated with a favorable response to ICI therapy. Importantly, metastatic melanoma patients with low PD-L1 expression in a lesion may also respond to ICI therapy (*12*). Therefore, immunohistochemistry PD-L1 expression on biopsies is not used in clinical practice to predict a patient's response to ICI therapy.

Discriminating between the different types of cells that may express PD-L1 in a metastatic melanoma lesion, such as malignant melanocytes, monocytes, and macrophages, may be important for ICI therapy response prediction (*21*). For example, pre-treatment PD-L1 expression on macrophages was associated with favorable response to ICI therapy, whereas pre-treatment PD-L1 expression on malignant melanocytes did not show any association with response (*22*). Although whole body PD-L1 PET cannot differentiate between the PD-L1 expression of different cellular compositions, it may be useful to visualize

PD-L1 expression in different lesions and predicting response per tumor lesion to ICI. Moreover, lesions with low PD-L1 expression on PET may indicate those lesions that need additional local treatment.

In our study, high 18F-BMS986192 uptake was observed in lymphoid tissues, such as the spleen and bone marrow. This is suggestive for PD-L1 targeting of the tracer 18F-BMS986192, as these organs contain high levels of PD-L1 expressing immune cells. Additionally, the follow-up 18F-BMS986192 PET scan showed an increased PD-L1 uptake in 2 patients with ICI-induced toxicity (thyroiditis and colitis), which may be a sign of inflammation with an increase in PD-L1 expressing immune cells.

The correlation of PD-L1 uptake in tumor lesions at baseline with response to treatment found in our study is comparable with a study in Non-Small Lung Cancer (NSCLC). That study demonstrated that both 18F-BMS-986192 (PD-L1) and 89Zr-Nivolumab(PD-1) PET imaging could predict response on a lesion-level (*13*). In addition, our study the second 18F-BMS986192 scan during ICI treatment at week 6 performed in four patients found an increased 18F-BMS986192 uptake correlating significantly with increased tumor size at follow-up at 12 weeks. This positive correlation can be explained by the fact that responding lesions have fewer PD-L1 expressing tumor cells, resulting in a reduction in 18F-BMS986192 uptake. On the other hand, a higher tracer uptake at week 6 in non-responding tumors at week 12 might theoretically be due to either a higher cell density or increased expression of PD-L1 per cell. PET cannot discriminate between these options. It is described that high PD L1 expressing tumor cells is related to a higher density of PD-1 tumor-associated T cells (*23*). Therefore, a delayed immune influx in PD-L1 upregulated tumor lesions at week 6 could be responsible for pseudoprogression at week 12. Unfortunately, our pilot study was unable to record any late response to immune checkpoint inhibition therapy as by that time these patients had already switched to another form of treatment. Moreover, technical aspects may have contributed to the correlation between the change in tumor size and the change in tracer uptake. A reduction in tumor size could also lead to a stronger partial volume effect (spill-out effect), which would also lead to the reduction in 18F-BMS986192 uptake.

Protein-based PET tracers targeting PD-L1 do not accumulate in normal brain tissue (*13*,*14*), because proteins usually cannot cross the intact blood-brain barrier. The inability of large proteins to enter the brain could be (part of) the cause of the mixed response of brain metastases to treatment with ICI. Brain metastases can disrupt the blood-brain barrier, but this is not always the case. Niemeijer et al. demonstrated that uptake of the protein-based PD-L1 tracers 18F-BMS-986192 and 89Zr-DFO-Nivolumab was observed in some, but not all, untreated brain metastases in two NSCLC patients (*13*). In our study, the 18F-BMS986192 uptake in brain metastases was also heterogeneous. Moreover, 18F-BMS986192 uptake in brain metastases showed a relation with response, although this correlation was not statistically significant, but this may be due to the sample size.

In this study, a 18F-labeled adnectin was used to target PD-L1 protein expression. In contrast to PET with the 89Zr-linked antibody tracer, 89Zr-DFO-Atezolizumab, 18F-BMS986192 PET provides the opportunity to acquire the PET scan 1 hour after tracer injection, and thus the examination can be completed within a single visit, which is highly convenient for the patient. Imaging on the same day as tracer injection is especially important for patients with brain metastases, where it is often essential to start treatment without delay. In addition, 18F-BMS986192 PET exposes the patients to a much lower radiation dose, which allows the acquisition of multiple 18F-BMS986192 PET examinations in the same patients within a short time frame. Moreover, it should be emphasized that the tumor accumulation of 18F-BMS986192 and most ^{89}Zr-labeled antibody tracers is based on slightly different mechanisms. 18F-BMS986192 uptake in the tumor is the result of reversible receptor binding and thus reflect receptor expression (*24*). The uptake of 89Zr-labeled antibody tracers, on the other hand, is the result of receptor binding, followed by receptor internalization, and thus represents receptor turnover, more than receptor expression. The lower radiation burden, the fast tracer kinetics and the uptake mechanism of 18F-BMS986192 make this tracer better suited for pharmacokinetics and pharmacodynamics studies than the 89Zr-labeled antibody tracers.

CONCLUSION

In conclusion, PET imaging with 18F-BMS986192 PET shows heterogeneous PD-L1 expression in brain and lung metastases of melanoma patients. The 18F-BMS986192 tumor uptake correlates with response on a per lesion basis with the same trend found in both intracerebral and extracerebral lesions. ICI-related toxicity can be detected at an early stage, before clinical symptoms appeared. The preliminary results of this pilot study warrant further evaluation of 18F-BMS986192 PET as a non-invasive imaging tool for assessment of PD-L1 expression in (brain) tumor lesions and prediction of ICI therapy response.

FINANCIAL DISCLOSURE

GH: Consulting and advisory role: Amgen, Roche, MSD, BMS, Pfizer, Novartis, Pierre Fabry; paid to the institution (UMCG). Research grant BMS, Seerave; paid to the institution (UMCG). No other potential conflicts of interest relevant to this article

MJ. Advisory role, paid to institution AstraZeneca, MSD

KEY POINTS

QUESTION: Is variability of PD-L1 PET tracer uptake in metastatic melanoma lesions related to tumor response on immune checkpoint inhibitors, particularly in brain metastases?

PERTINENT FINDINGS: In this pilot study, 18F-BMS986192 PET showed heterogeneous uptake in intra and extracerebral metastatic lesions in melanoma patients. Baseline 18F-BMS986192 uptake was able to predict an immune checkpoint inhibitor-induced reduction in lesion volume.

IMPLICATIONS FOR PATIENT CARE: In melanoma patients, PD-L1 PET imaging may identify which metastatic lesions require local treatment in addition to immune checkpoint inhibitors.

REFERENCES

1. Ascierto PA, Long GV, Robert C, et al. Survival Outcomes in Patients with Previously Untreated BRAF Wild-Type Advanced Melanoma Treated with Nivolumab Therapy: Three-Year Follow-up of a Randomized Phase 3 Trial. *JAMA Oncol*. 2019;5:187-194.
2. Robert C, Long GV, Brady B, et al. Nivolumab in Previously Untreated Melanoma without BRAF Mutation. *N Engl J Med*. 2015;372:320-330.
3. Topalian SL, Sznol M, McDermott DF, et al. Survival, durable tumor remission, and long-term safety in patients with advanced melanoma receiving nivolumab. *J Clin Oncol*. 2014;32:1020-1030.
4. Weber JS, D'Angelo SP, Minor D, et al. Nivolumab versus chemotherapy in patients with advanced melanoma who progressed after anti-CTLA-4 treatment (CheckMate 037): A randomised, controlled, open-label, phase 3 trial. *Lancet Oncol*. 2015;16:375-384.
5. Schachter J, Ribas A, Long G V, et al. Pembrolizumab versus ipilimumab for advanced melanoma: final overall survival results of a multicentre, randomised, open-label phase 3 study (KEYNOTE-006). *Lancet*. 2017;390:1853-1862.
6. Ascierto PA, Del Vecchio M, Robert C, et al. Ipilimumab 10 mg/kg versus ipilimumab 3 mg/kg in patients with unresectable or metastatic melanoma: a randomised, double-blind, multicentre, phase 3 trial. *Lancet Oncol*. 2017;18:611-622.
7. Robert C, Thomas L, Bondarenko I, et al. Ipilimumab plus Dacarbazine for Previously Untreated Metastatic Melanoma. *N Engl J Med*. 2011;364:2517-2526.
8. Hodi FS, Chiarion-Sileni V, Gonzalez R, et al. Nivolumab plus ipilimumab or nivolumab alone versus ipilimumab alone in advanced melanoma (CheckMate 067): 4-year outcomes of a multicentre, randomised, phase 3 trial. *Lancet Oncol*. 2018;19:1480-1492.
9. Wolchok JD, Hoos A, O'Day S, et al. Guidelines for the evaluation of immune therapy activity in

solid tumors: Immune-related response criteria. *Clin Cancer Res*. 2009;15:7412-7420.

10. Blankenstein SA, Aarts MJB, van den Berkmortel FWPJ, et al. Surgery for Unresectable Stage IIIC and IV Melanoma in the Era of New Systemic Therapy. *Cancers (Basel)*. 2020;12:1176.
11. Noh T, Walbert T. Brain metastasis: clinical manifestations, symptom management, and palliative care. *Handb Clin Neurol*. 2018;149:75-88.
12. Santos-Briz A, Cañueto J, Carmen S del, et al. Value of PD-L1, PD-1, and CTLA-4 Expression in the Clinical Practice as Predictors of Response to Nivolumab and Ipilimumab in Monotherapy in Patients With Advanced Stage Melanoma. *Am J Dermatopathol*. 2021;43:423-428.
13. Niemeijer AN, Leung D, Huisman MC, et al. Whole body PD-1 and PD-L1 positron emission tomography in patients with non-small-cell lung cancer. *Nat Commun*. 2018;9:1-5.
14. Bensch F, van der Veen EL, Lub-de Hooge MN, et al. 89Zr-atezolizumab imaging as a non-invasive approach to assess clinical response to PD-L1 blockade in cancer. *Nat Med*. 2018;24:1852-1858.
15. Eisenhauer EA, Therasse P, Bogaerts J, et al. New response evaluation criteria in solid tumours: Revised RECIST guideline (version 1.1). *Eur J Cancer*. 2009;45:228-247.
16. Donnelly DJ, Adam Smith R, Morin P, et al. Synthesis and biologic evaluation of a novel 18 F-labeled adnectin as a PET radioligand for imaging PD-L1 expression. *J Nucl Med*. 2018;59:529-535.
17. Kaalep A, Sera T, Oyen W, et al. EANM/EARL FDG-PET/CT accreditation - summary results from the first 200 accredited imaging systems. *Eur J Nucl Med Mol Imaging*. 2018;45:412-422.
18. Boellaard R, Delgado-Bolton R, Oyen WJGG, et al. FDG PET/CT: EANM procedure guidelines for tumour imaging: version 2.0. *Eur J Nucl Med Mol Imaging*. 2015;42:328-354.
19. Hofheinz F, Bütof R, Apostolova I, et al. An investigation of the relation between tumor-to-liver ratio (TLR) and tumor-to-blood standard uptake ratio (SUR) in oncological FDG PET. *EJNMMI Res*. 2016;6:19.
20. Persigehl T, Lennartz S, Schwartz LH. IRECIST: How to do it. *Cancer Imaging*. 2020;20:1-7.

21. Tang F, Zheng P. Tumor cells versus host immune cells: whose PD-L1 contributes to PD-1/PD-L1 blockade mediated cancer immunotherapy? *Cell Biosci*. 2018;8:34.

22. Toki MI, Merritt CR, Wong PF, et al. High-plex predictive marker discovery for melanoma immunotherapy-treated patients using digital spatial profiling. *Clin Cancer Res*. 2019;25:5503-5512.

23. Kandl TJ, Sagiv O, Curry JL, et al. High expression of PD-1 and PD-L1 in ocular adnexal sebaceous carcinoma. *https://doi.org/101080/2162402X20181475874*. 2018;7.

24. Stutvoet TS, van der Veen EL, Kol A, et al. Molecular Imaging of PD-L1 Expression and Dynamics with the Adnectin-Based PET Tracer ^{18} F-BMS-986192. *J Nucl Med*. 2020;61:1839-1844.

FIGURES WITH LEGENDS

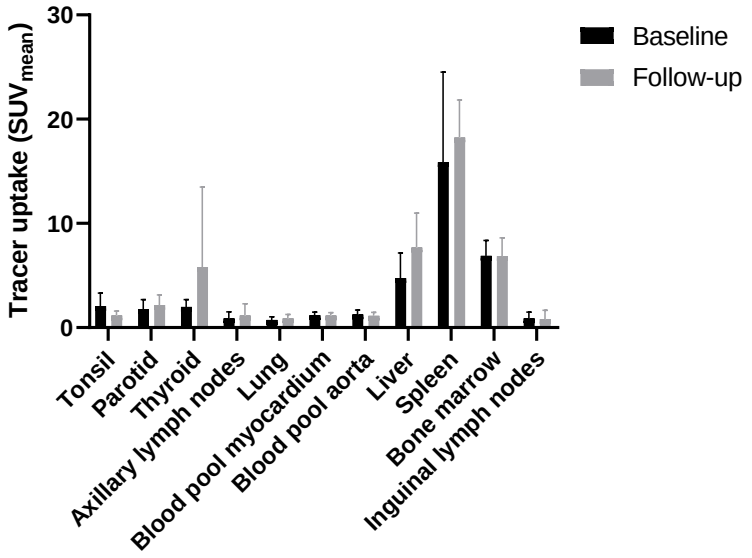

Figure 1. Biodistribution of 18F-BMS986192 at baseline (n=8) and follow-up (n=4). In the patients with follow-up scans, 18F-BMS986192 uptake in the tonsil was significantly higher at baseline than at follow up (Wilcoxon signed rank test, p=0.002). There were no other differences in 18F-BMS986192 uptake between baseline and follow up.

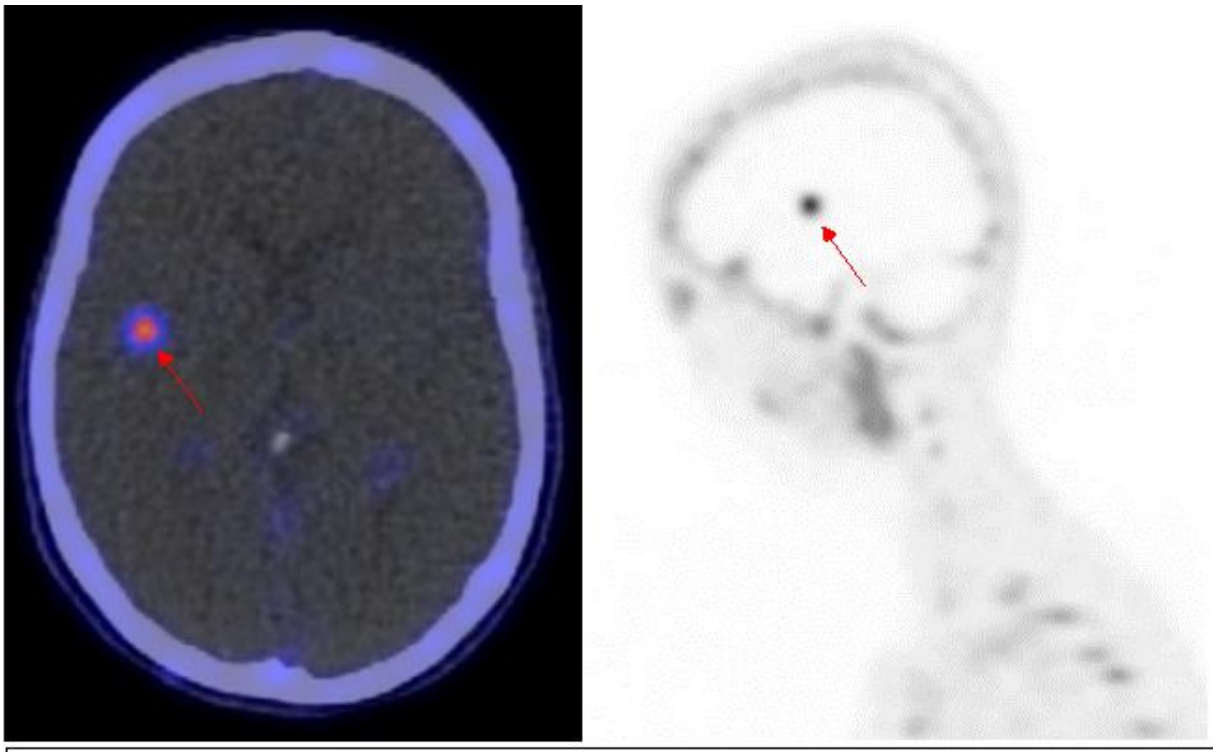

SUV_{max}	4.16	SUV_{peak}	2.02
SUV_{mean}	1.84	TBR	1.59

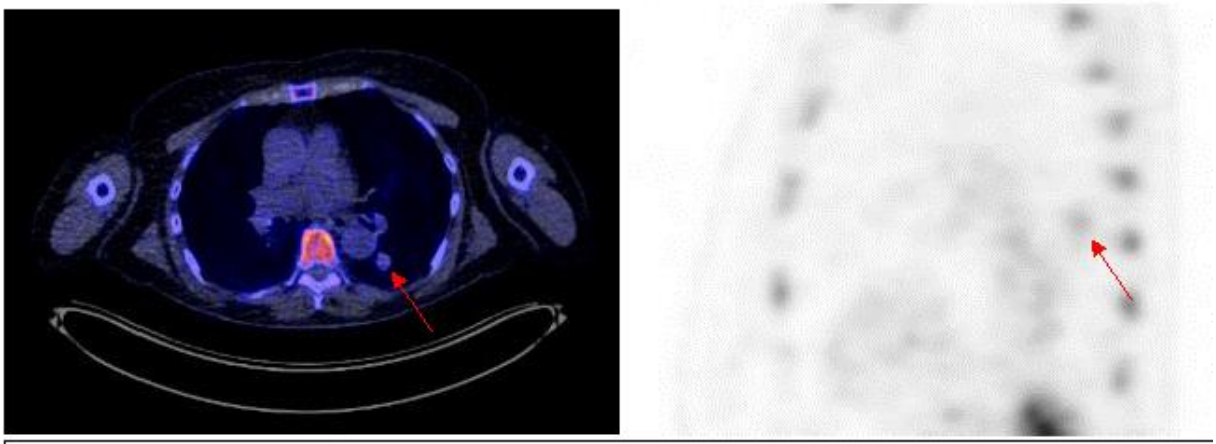

SUV_{max}	1.68	SUV_{peak}	1.29
SUV_{mean}	1.84	TBR	1.39

Figure 2. Examples of a brain lesion (above) and a lung lesion (below). Fused PET/CT transverse images and PET saggital images are shown. Semiquantitative measurements are reported underneath the images. Target-to-background ratio (TBR) is calculated as the lesion SUVpeak divided by the SUVmean in the aortic blood pool.

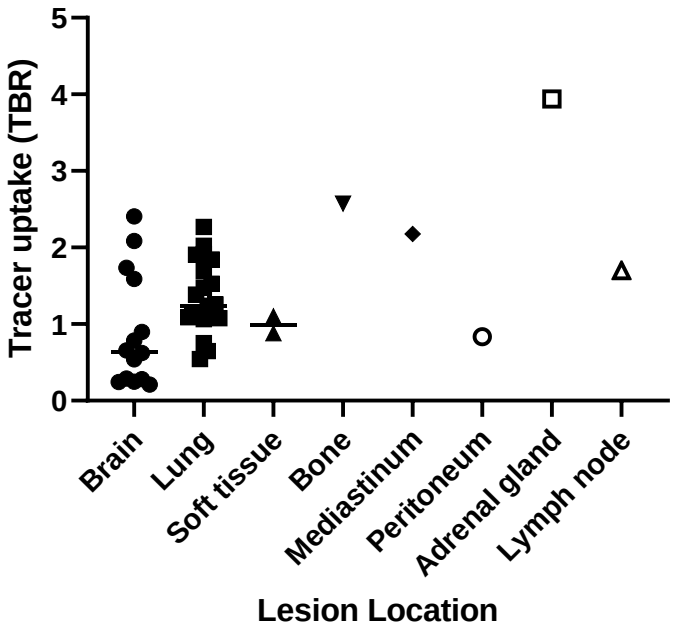

Figure 3. Baseline 18F-BMS986192 tracer uptake measured as a target-to-background ratio (TBR) derived from the SUV_{peak} of the lesion and SUV_{mean} of the aortic blood pool. Median group value is reported as a line. No significant difference was found between the mean values of the brain and lung lesions (Mann-Whitney U test, p = 0.06). Analysis included 42 tumor lesions (21 lung, 14 brain, 2 soft tissue, 1 bone, mediastinum, peritoneum, adrenal gland, and lymph node lesions) in 8 patients.

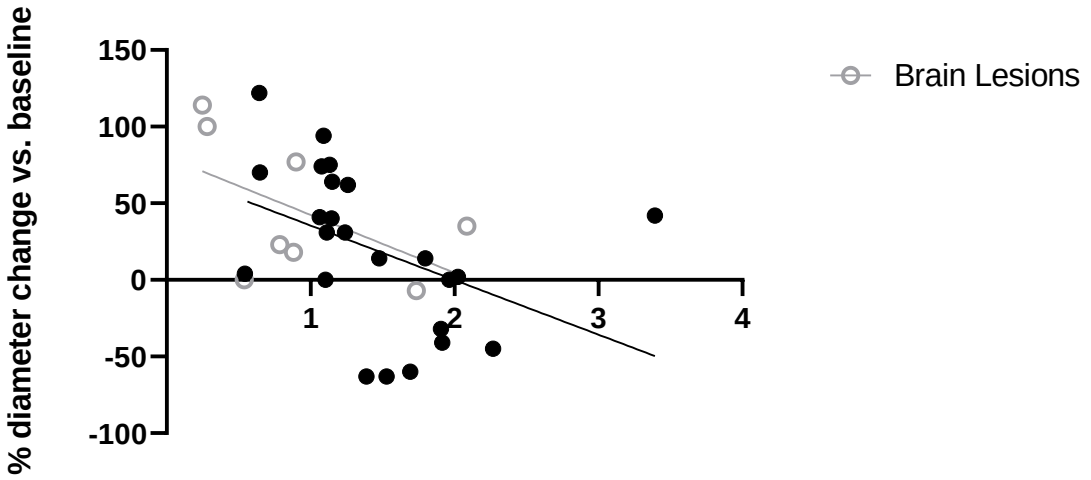

Figure 4. Association of target-to-background ratio (TBR), derived from the SUV_{peak} of the lesion and SUV_{mean} of the aortic blood pool, and the relative (%) diameter change of the lesions (Spearman's rank, r= -0.43, p= 0.014). From all eight patients, only lesions larger than 10mm at baseline were included in this analysis (n=32). Brain lesions are shown as open circles (n=8).

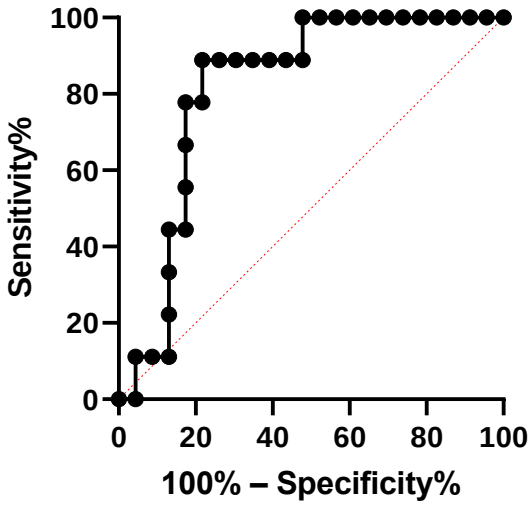

Figure 5. ROC curve of the tumor-to-blood ratio (TBR) of the lesion, showing the sensitivity and specificity for discriminating between tumors increasing or decreasing in diameter. The area under the curve is 0.82 (p=0.006).

A

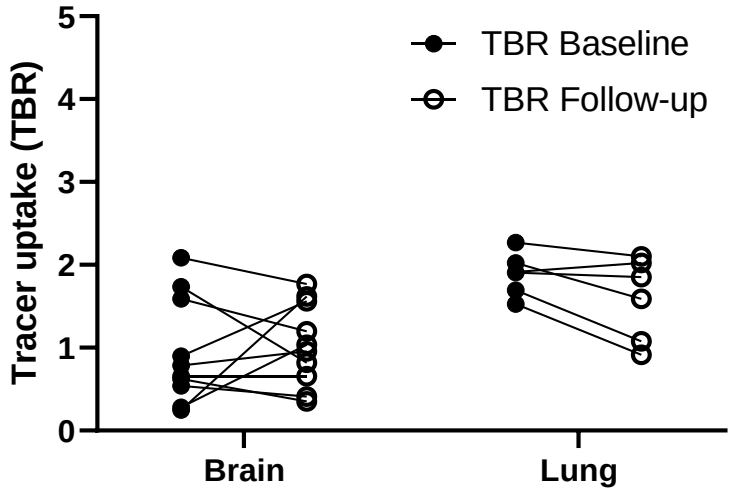

B

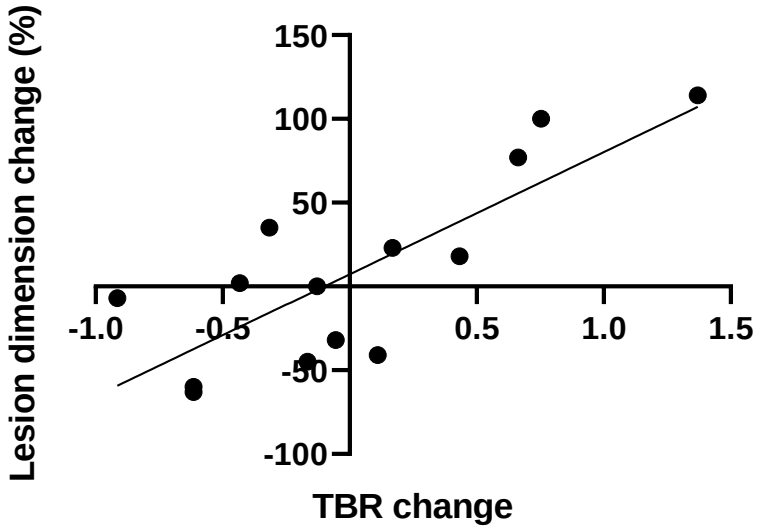

Figure 6. (A) 18F-BMS986192 uptake for brain and lung lesions at baseline and follow up (4 patients, 16 lesions). Tracer uptake is reported as a tumor-to-blood ratio (TBR). Significant differences in tracer uptake were observed between brain and lung lesions, both at baseline and at follow up (Wilcoxon signed rank test, p=0.004 and p=0.05, respectively). (B) Association between the change in lesion size and the change in the tumor-to-blood ratio (TBR) of the follow up 18F-BMS986192 scan compared to baseline ($TBR_{follow\ up}$ – $TBR_{baseline}$) (4 patients, 14 lesions). A significant positive correlation was found between increasing TBR and increasing lesion diameter (Spearman's rank, r=0.79, p=0.0007).

Thyroid Right Lobe	
SUV_{max}	4.18
SUV_{peak}	3.21
SUV_{mean}	3.39
TBR	2.26
Thyroid Left Lobe	
SUV_{max}	2.66
SUV_{peak}	2.01
SUV_{mean}	1.77
TBR	1.42

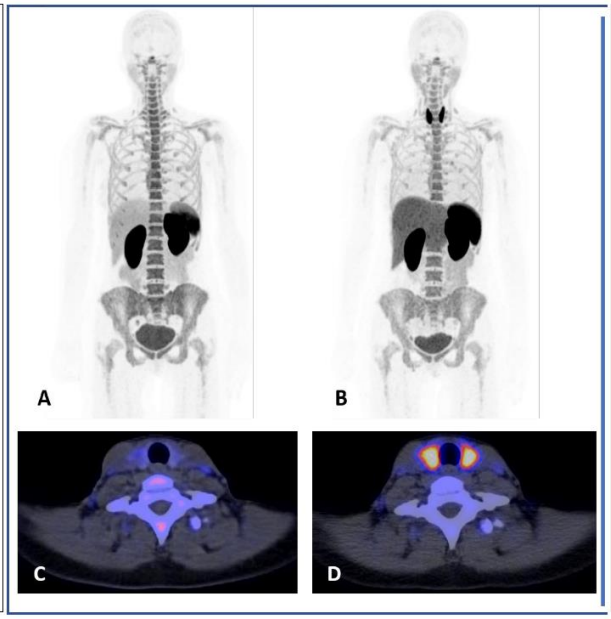

Thyroid Right Lobe	
SUV_{max}	19.93
SUV_{peak}	16.87
SUV_{mean}	14.68
TBR	12.98
Thyroid Left Lobe	
SUV_{max}	21.94
SUV_{peak}	16.17
SUV_{mean}	13.74
TBR	12.44

Figure 7. 18F-BMS986192 -L1 PET/CT scans of two patients who developed ICI-related toxicity. Images A-D show 18F-BMS986192 scans of a patient who developed ICI-related thyroiditis with increased uptake on treatment (B,D) compared to baseline (A,C). Semiquantitative measurements are shown for the basline scan (left) and the follow up scan (right). Target-to-background ratio (TBR) was calculated by dividing the thyroid SUVpeak by the SUVmean in the aortic blood pool.

TABLES

Table 1. Patient Characteristics. *Including 6 patients with brain metastases; **Lesions that were detected at baseline and follow up by MR or CT imaging.

Number of patients included	**10**
Number of evaluable patients*	**8**
Number of lesions on PET	**47**
Number of evaluable lesions**	**42**
Number of lesions ≥10 mm at baseline (CT or MRI)	**32**
Median patient age at baseline (years)	**62**
Number of females, n (%)	**3 (38)**
Number of PET scans per patient, n (%)	
- **1**	**4 (50)**
- **2**	**4 (50)**
Immunotherapy regimen, n (%)	
- **Anti-CTLA4 + Anti-PD-1**	**5 (62)**
- **Anti-PD1**	**3 (38)**
Number of patients by treatment response (RECIST v.1.1), n (%)	
- **Complete response**	**0 (0)**
- **Partial response**	**2 (25)**
- **Stable disease**	**2 (25)**
- **Progressive disease**	**4 (50)**

SUPPLEMENTAL MATERIAL

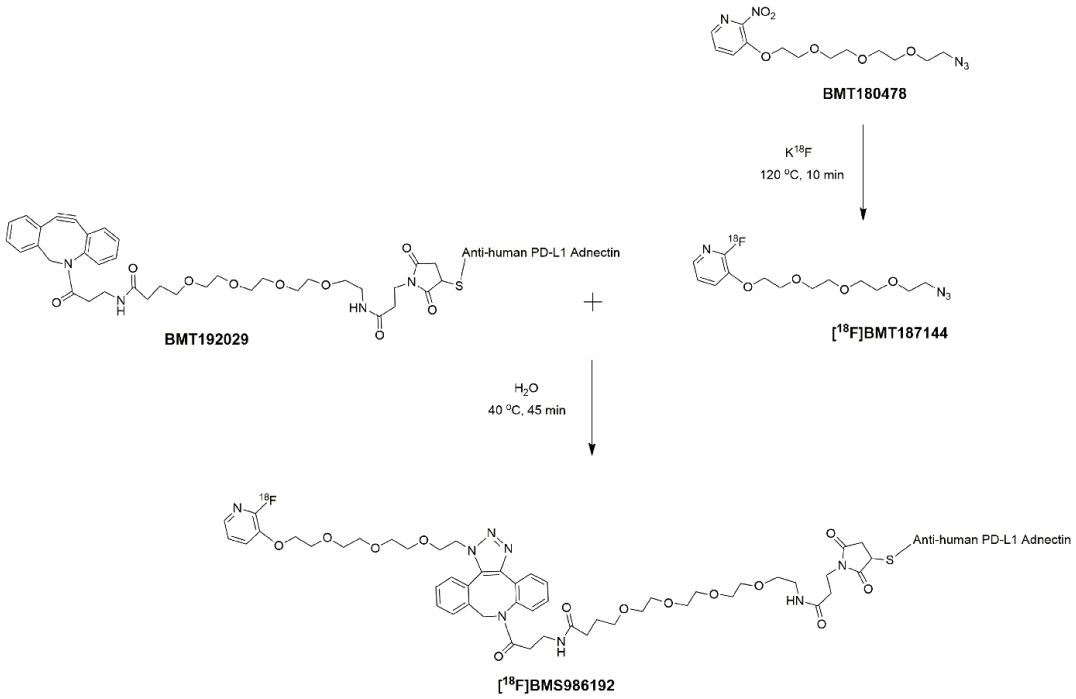

Supplemental Figure 1. Schematic representation of the synthesis of 18F-BMS986192.

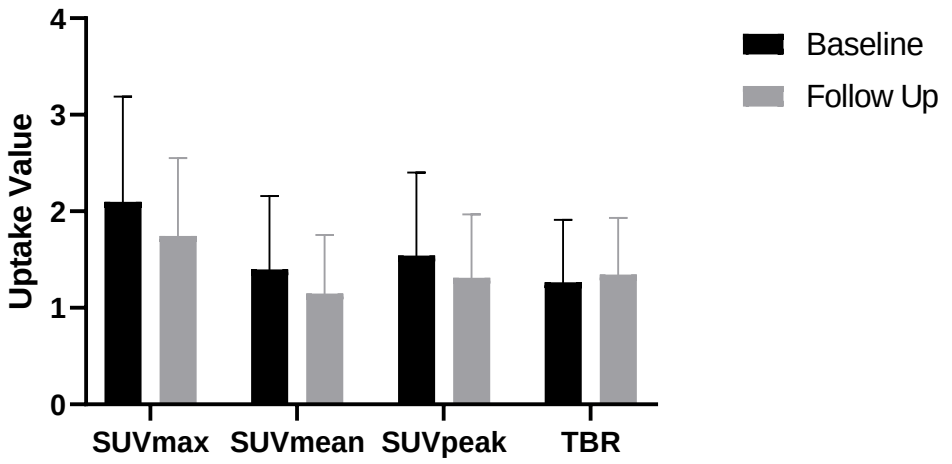

Supplemental Figure 2. 18F-BMS986192 tracer uptake at baseline and follow up using four uptake parameters: SUV_{max}, SUV_{mean}, SUV_{peak}, and a tumor-to-blood ratio (TBR) derived from the tumour SUV_{peak} and the aortic blood pool SUV_{mean} (4 patients, 19 lesions).

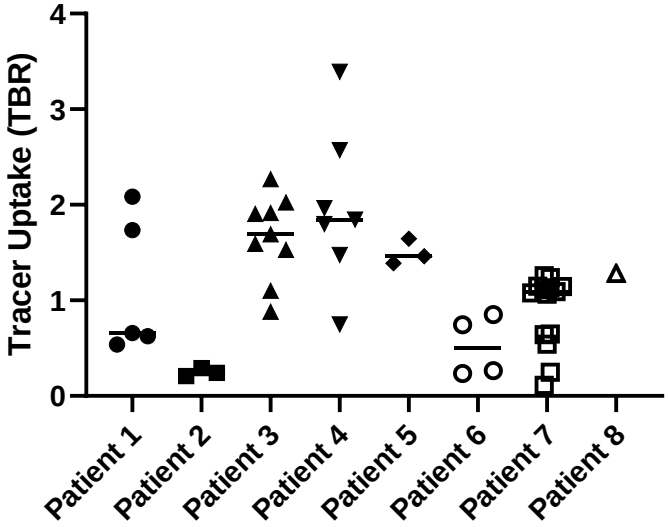

Supplemental Figure 3A. 18F-BMS986192 tracer uptake at baseline as tumor-to-blood ratio (TBR) derived from the tumour SUV_{peak} and the aortic blood pool SUV_{mean}. Data shown for all included patients in this study and shows 42 lesions.

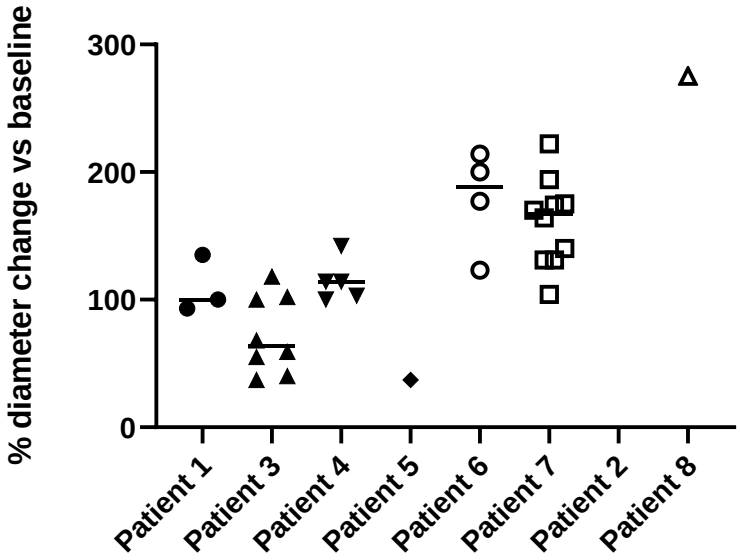

Supplemental Figure 3B. The diameter change during ICI therapy compared to baseline of tumor lesions per patient. Data shown for all included patients in this study and shows 32 lesions. Patient 2 only had lesions that were smaller than 1 cm at baseline and, therefore, had no response evaluable lesions.

GRAPHICAL ABSTRACT